

Assembly and melting of DNA nanotubes from single-sequence tiles

T L Sobey^{1,2}, S Renner¹ and F C Simmel¹

¹ Lehrstuhl für Bioelektronik-E14, Department Physik, Technische Universität München, James-Franck-Straße, D-85748 Garching, Germany

² Department Physik, Ludwig-Maximilians-Universität München, Geschwister-Scholl-Platz 1, D-80539 München, Germany

E-mail: thomas.sobey@ph.tum.de

Received 3 June 2008, in final form 25 August 2008

Published 17 December 2008

Online at stacks.iop.org/JPhysCM/21/034112

Abstract

DNA melting and renaturation studies are an extremely valuable tool to study the kinetics and thermodynamics of duplex dissociation and reassociation reactions. These are important not only in a biological or biotechnological context, but also for DNA nanotechnology which aims at the construction of molecular materials by DNA self-assembly. We here study experimentally the formation and melting of a DNA nanotube structure, which is composed of many copies of an oligonucleotide containing several palindromic sequences. This is done using temperature-controlled UV absorption measurements correlated with atomic force microscopy, fluorescence microscopy and transmission electron microscopy techniques. In the melting studies, important factors such as DNA strand concentration, hierarchy of assembly and annealing protocol are investigated. Assembly and melting of the nanotubes are shown to proceed via different pathways. Whereas assembly occurs in several hierarchical steps related to the formation of tiles, lattices and tubes, melting of DNA nanotubes appears to occur in a single step. This is proposed to relate to fundamental differences between closed, three-dimensional tube-like structures and open, two-dimensional lattices. DNA melting studies can lead to a better understanding of the many factors that affect the assembly process which will be essential for the assembly of increasingly complex DNA nanostructures.

(Some figures in this article are in colour only in the electronic version)

1. Introduction

Duplex formation between DNA strands with complementary base sequences is one of the most prominent examples for molecular recognition in biochemistry. In a non-biological context, base-pairing interactions between artificially designed DNA molecules have been used for the construction of nanoscale objects, devices [1] and molecular lattices [2–4], culminating in the recent experimental demonstration of DNA origami by Shih *et al* [5] and Rothemund [6]. In contrast to typical biological structures, DNA nanostructures are composed of many short oligonucleotides which associate with each other according to an assembly plan encoded in their sequences. The assembly of such structures is usually accomplished by careful thermal annealing from 95 °C to room temperature.

The thermodynamics of duplex association and melting has been studied in great detail essentially since the elucidation of the structure of DNA. A brief discussion on this follows, describing what has been done and why theoretical advances are of limited use in describing the assembly and melting processes of the DNA nanotubes studied here. This is followed by a description of the system we study.

Theoretical advances in thermodynamics of nucleic acids began with analysing the secondary structure of single molecules. The secondary structure of a nucleic acid strand in a particular physical conformation is simply the set of base pairs present in the molecule. Computational analysis of minimum free energy secondary structure has developed considerably and involves dynamic programming techniques [7]. The partition function for short subsequences is calculated and iteratively longer sequences are considered until the full

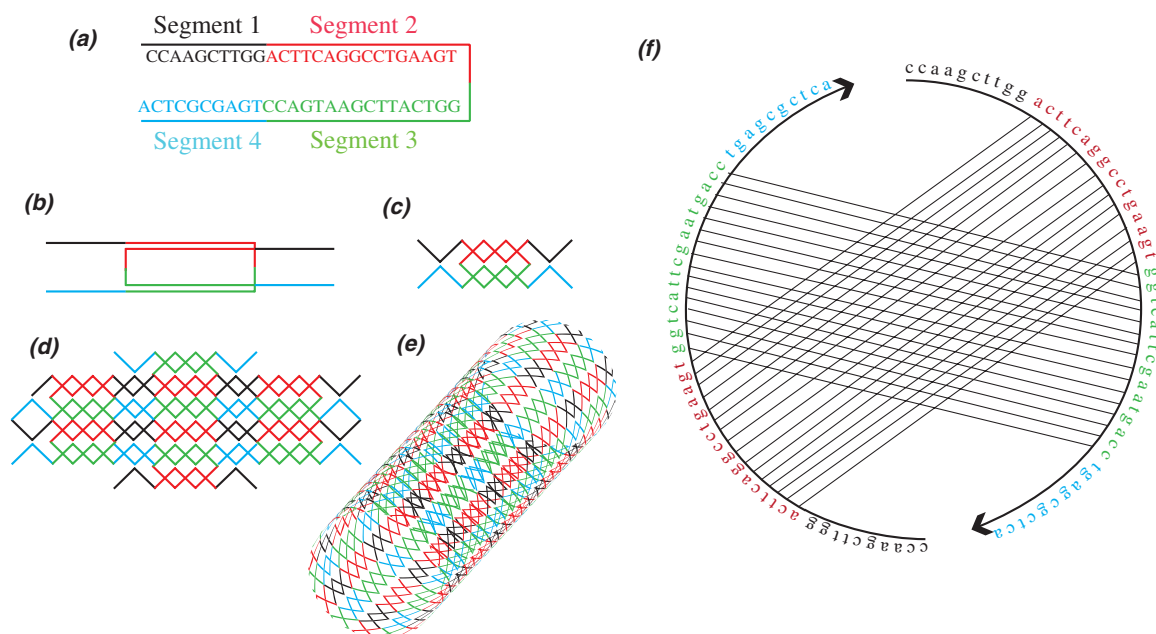


Figure 1. Assembly of a DNA nanotube from many copies of a single sequence developed by Mao *et al* [20]. (a) The sequence consisting of four palindromic segments (segments that are self-complementary). These are called segment 1, 2, 3 and 4 in this study. (b), (c) Two copies of this sequence bind at segment 2 and 3 to create two double helices that cross-over in two positions. This leaves four single-stranded ends from this ‘tile’. The double helices are 16 base-pairs long. (d) These single-stranded ends are 10 bases long and can bind (at lower temperatures because they are shorter than the 16 base-pair helices above) to others in the solution. Segment 4 will bind to other segment 4s because these are designed to be self-complementary, likewise with the segment 1s. This forms a ‘lattice’. (e) These lattices can bind into DNA nanotubes in an intracomplex process. (f) A polymer graph of the double crossover tile structure represented in (b) and (c). The crossing lines representing the base pairing indicate that this structure is a pseudoknot. ((a)–(d) adapted from Liu *et al* [20].)

partition function is obtained. This can be used within certain limits to calculate the equilibrium probability of any secondary structure.

Accurate prediction of DNA secondary structure, hybridization and melting using dynamic programming algorithms require databases of thermodynamic parameters. Such databases have been developed empirically by multiple groups including SantaLucia and colleagues [8, 9], Breslauer and colleagues [10] and many others.

Development of multi-strand nucleic acid problems have only occurred recently, with work by Zuker and colleagues [11], Condon and colleagues [12], and Pierce and colleagues [7, 13, 14]. However, these works are limited to systems without pseudoknots. Nucleic acid structures can be represented as polymer graphs, with the strands drawn along the circumference of a circle and base pairs depicted on straight lines joining complementary bases. Pseudoknots correspond to polymer graphs with crossing lines. These can be particularly difficult to analyse. The first structure thought to form from the DNA nanotube sequence studied here (discussed further below) is depicted in figure 1(b) and shown as a polymer graph in figure 1(f). The pseudoknot indicates that despite the significant advances in thermodynamics and structural theory, limited help is available to analyse the nanotube strand (and many other recently developed structures) in this study.

Rather than making *ab initio* calculations many researchers have fitted experimental data to standard thermodynamic and kinetic theories. Schulman and Winfree have

demonstrated control over nucleation and growth processes using systematic design of self-assembled ribbons. A seed molecule initiates growth of a structure, but this growth is kinetically inhibited in the seed’s absence. This allows for proper initiation of algorithmic crystal growth [15]. Niemeyer and colleagues used Förster resonant energy transfer (FRET) studies to monitor in real-time the self-assembly of DNA tiles and lattices. This allows calculation of thermodynamic parameters of the assembled structures [16]. Using fluorescence microscopy Fygenon and colleagues have shown that DNA nanotubes can join end-to-end to make longer nanotubes as well as split into parts. Also, by using ligating enzymes to join the ends of DNA strands, they managed to increase the thermal stability of DNA nanotubes [17, 18].

We have recently shown that it is possible to self-assemble DNA origami structures isothermally, by replacing temperature annealing procedures with dilution of denaturing agents (agents that act to break the hydrogen bonds between base pairs) [19]. An analysis of the thermodynamics and kinetics occurring during this process is in progress.

In the present paper we take an alternative approach to those techniques discussed above. We study formation and melting of DNA self-assemblies by making detailed UV absorption measurements of temperature-controlled DNA solutions and correlate these with atomic force microscopy and fluorescence microscopy observations. This provides new insights into the formation and melting that demonstrate the hierarchy of the dynamic assembly process.

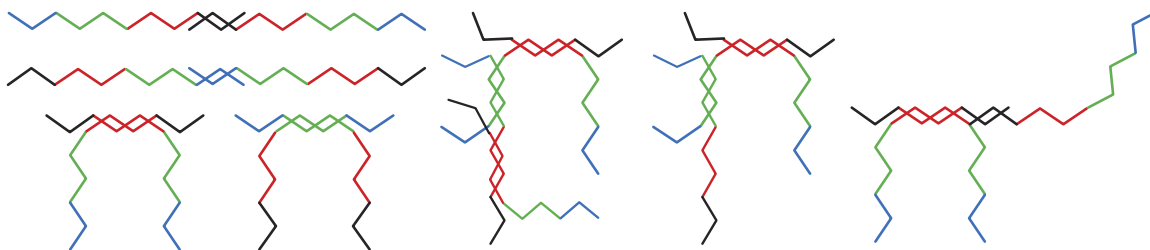


Figure 2. Many other complexes are possible apart from the double-stranded-crossover tiles and regular lattice. Some are depicted here. However, these may result in either more single-stranded segments or structures with larger stress.

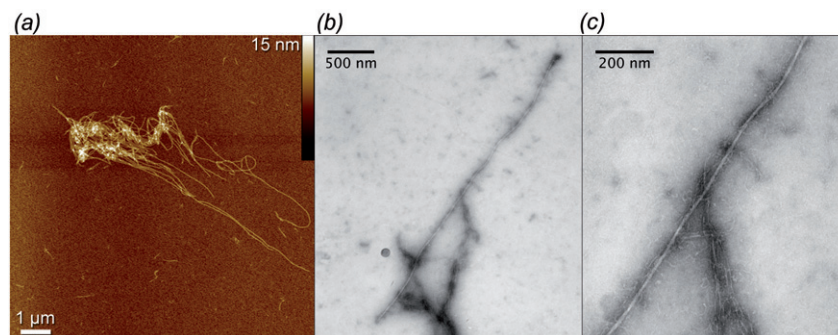


Figure 3. (a) An atomic force microscopy image of aggregated DNA nanotubes. Scale bar is $1 \mu\text{m}$, height scale is 15 nm . Individual nanotubes have a diameter of approximately $7 \pm 2 \text{ nm}$, as measured by topographic height. (b) Transmission electron microscopy images of a DNA nanotube. Scale bar is 500 nm . The irregular dark area in the lower part of the image is thought to be DNA lattice and tiles that have not successfully formed nanotubes. (c) Magnified image of the middle section of the previous image. Scale bar is 200 nm : measured width of the nanotube is $8 \pm 3 \text{ nm}$ and measured length is $3.48 \pm 0.2 \mu\text{m}$. Observed fine (white) structure thinner than the nanotube is thought to be chains of tiles.

In particular, we study a very elegant single-sequence nanotube structure introduced by Mao and colleagues [20]. This structure was chosen due to its apparently simple assembly process: in Mao's approach, a single 52-nucleotide (nt) long DNA strand is designed such that it forms a double crossover structure with itself (figure 1). The strand consists of four palindromic segments. These are called segments 1, 2, 3 and 4 in this study. A sequence is palindromic if it is equal to its complementary sequence in the reverse direction—it is self-complementary. Each crossover is anti-parallel, that is the strands reverse direction. The double helix segments are 16 base pairs long (i.e. the length of segments 2 and 3): this is approximately 1.5 helix turns, or an odd number of half-turns (10.5 base pairs per helix in relaxed B DNA). This structure is known as a tile (of type DAO [21]), for reasons that will become obvious.

These tiles have four single-stranded DNA ends—two each of segments 1 and 4. These ends bind to the complementary ends of other tiles, and under slow annealing conditions ordered lattices of tiles will form.

Many configurations of this strand are possible. Some—other than the tile described—are depicted in figure 2. However, these structures always result in unbound single-stranded DNA, or in structures that are not at the minimum free energy. Thus with slow annealing (attempting to stay within dynamic equilibrium conditions), the ordered tile lattice will preferentially form.

This lattice is flexible, particularly as there are nicks in double-stranded DNA where tiles join one another. As the lattices form, free tile and lattice concentrations decrease (larger lattices resulting in fewer numbers of lattices) and intra-lattice interaction becomes more likely than inter-lattice interaction and tubes (helical or non-helical) are able to form.

An atomic force microscopy (AFM) image of aggregated DNA nanotubes on a mica surface is shown in figure 3(a). These were annealed over 48 h. The individual tubes have diameters of approximately $7 \pm 2 \text{ nm}$ (as measured by topographic height, which minimized the influence of AFM tip convolution) and lengths of $\sim 20 \mu\text{m}$, although this is dependent primarily on annealing times and is discussed in the results section. In figures 3(b) and (c), transmission electron microscopy images of a single nanotube are shown from a solution annealed over 12 h. In (b), the whole nanotube of measured length $3.48 \pm 0.2 \mu\text{m}$ is imaged, while in (c) at higher magnification a section of it is imaged. Its measured width is $8 \pm 3 \text{ nm}$, agreeing within error with that measured from the AFM.

Many different versions of DNA nanotubes requiring differing numbers of DNA strands and differing DNA sequences have been experimentally realized [22–28]. We choose to study this particular sequence because of its inherent simplicity based on symmetry, resulting in only one sequence being required. This removes problems of stoichiometry. However, despite its simplicity, a rich variety of thermodynamic behaviour was observed.

The nanotubes studied here have already been demonstrated as a useful link between bottom-up self-assembly and top-down nanolithography approaches. Yan and colleagues [29] have used biotin–streptavidin binding to organize quantum dots along the nanotubes, and followed this with PDMS (polydimethylsiloxane) stamping to create large-area (at least tens of microns squared) ordered arrays of these structures.

Increasing our understanding of the formation and assembly dynamics should lead to better control of yields and optimized formation times. Furthermore, it is expected to result in better control of the nanotube lengths and their variability.

2. Experimental details

2.1. DNA

DNA oligonucleotides were purchased from Biomers.net (Ulm, Germany) with HPLC purification and in a lyophilized state. These were dissolved in $1 \times$ TE buffer (pH 8, Sigma-Aldrich, Germany) and diluted to $100 \mu\text{M}$ concentration, as measured by UV absorption at 260 nm at room temperature on a Nanophotometer (Implen GmbH, Munich, Germany). The DNA sequences used were:

Standard DNA nanotube strand:

5' cca agc ttg gac ttc agg cct gaa gtg gtc att cga atg acc tga gcg ctc a 3'

Segment 1:

5' cca agc ttg g 3'

Segment 2:

5' act tca ggc ctg aag t 3'

Segment 3:

5' ggt cat tcg aat gac c 3'

Segment 4:

5' tga gcg ctc a 3'

Modified strand with non-complementary ends:

5: 5' cac cgc aaa tac ttc agg cct gaa gtg gtc att cga atg acc aaa gcc gtc t 3'.

An additional DNA sequence that was fluorescein-labelled at the 5'-end was purchased from Integrated DNA Technologies (Leuven, Belgium) with HPLC purification and dissolved as previously:

5' FAM cca agc ttg gac ttc agg cct gaa gtg gtc att cga atg acc tga gcg ctc a 3'.

For each experiment, the desired DNA sequence was diluted to $1 \mu\text{M}$ in $1 \times$ TAE (tris-acetate-ethylenediamine tetraacetic acid, pH 8) 12.5 mM MgCl_2 buffer. This buffer was pre-filtered using $0.2 \mu\text{m}$ syringe filters (surfactant-free cellulose acetate, Nalgene Nunc Inc, New York, USA). Pipette tips were cut short when working with nanotube solutions, making a wider opening in order to minimize damage to the nanotubes.

2.2. UV spectrometry

The 260 nm absorption peak of DNA was measured using a UV–vis spectrophotometer (V550, Jasco, Groß-Umstadt, Germany) and heating was provided by a Peltier element

stabilized by contact with a temperature-controlled water bath (MP/F-25, Julabo Labortechnik GmbH, Seelbach, Germany). The water bath was programmed at a constant 25°C . The sample solution was loaded into a screw-top cuvette (#117.104, Hellma GmbH, Muellheim, Germany), making certain that the cuvette was completely full ($2700 \mu\text{l}$) and the screw-top was closed firmly. This ensured that upon heating no bubbles formed in the solution. A 5 nm bandwidth excitation was used. The temperature-control program was written in the macro language of the provided Jasco software (Spectra Manager 1). Typically, a sample was cooled from 95 to 85°C at a rate of 30°C h^{-1} (in order to minimize damage to the DNA), and then at a slower rate of 6°C h^{-1} to 20°C . Measurements were taken from an analogue 0 – 1 V output and recorded using a self-programmed Labview module. Measurements were made once a second. Data was processed using Igor Pro 6 software (Wavemetrics Inc., Nimbus, USA). Measurements were median smoothed over 100 data points and typical measurements had tens of thousands to hundreds of thousands of data points. Curves were fitted with high order polynomials to allow numerical differentiation without interference from noise.

2.3. Atomic force microscopy

Samples were imaged in tapping mode using a Multimode AFM with Nanoscope IIIa controller and E-scanner (Veeco Instruments, Santa Barbara, USA). Imaging was performed in TAE/ Mg^{2+} buffer solution with NP-S oxide-sharpened silicon nitride cantilevers (Veeco Probes, Camarillo, USA) using resonance frequencies between 7 and 9 kHz of the narrow $100 \mu\text{m}$, 0.38 N m^{-1} force constant cantilever. $5 \mu\text{l}$ of sample solution was dropped onto a freshly cleaved mica surface (Plano, Dresden, Germany) glued to a metal puck (Plano). After another 30 s , $30 \mu\text{l}$ of additional buffer solution was added to the sample. After engaging the tip on the surface, imaging parameters were optimized for best image quality while maintaining the highest possible setpoint to minimize damage to the samples. Images were post-processed by subtracting a second-order polynomial from each scan line. Drive amplitudes were approximately 0.45 V , integral gains approximately 0.15 and proportional gains approximately 0.3 .

2.4. Fluorescence microscopy

Fluorescently labelled DNA was mixed with the normal DNA strand at a ratio of $1:3$ and a DNA nanotube solution was prepared as per the protocol for the UV spectrophotometer. $10 \mu\text{l}$ of solution was filled into a hole of 5 mm diameter in a 1 mm thick polydimethylsiloxane (PDMS) spacer between two coverslips. This was mounted on a temperature-controlled stage of an inverted fluorescence microscope (IX71, Olympus, Germany). The temperature was measured with a calibrated Pt100 sensor which was glued directly onto one of the coverslips with heat conducting paste, and the heating power was controlled by LabView software. The temperature at the Pt100 sensor was accurate to within 0.5°C . Observations were made using a $10\times$ objective and 460 – 495 nm excitation/ 510 nm emission filter (U-MWIBA2, Olympus). Images were captured using a CCD camera (Coolsnap HQ,

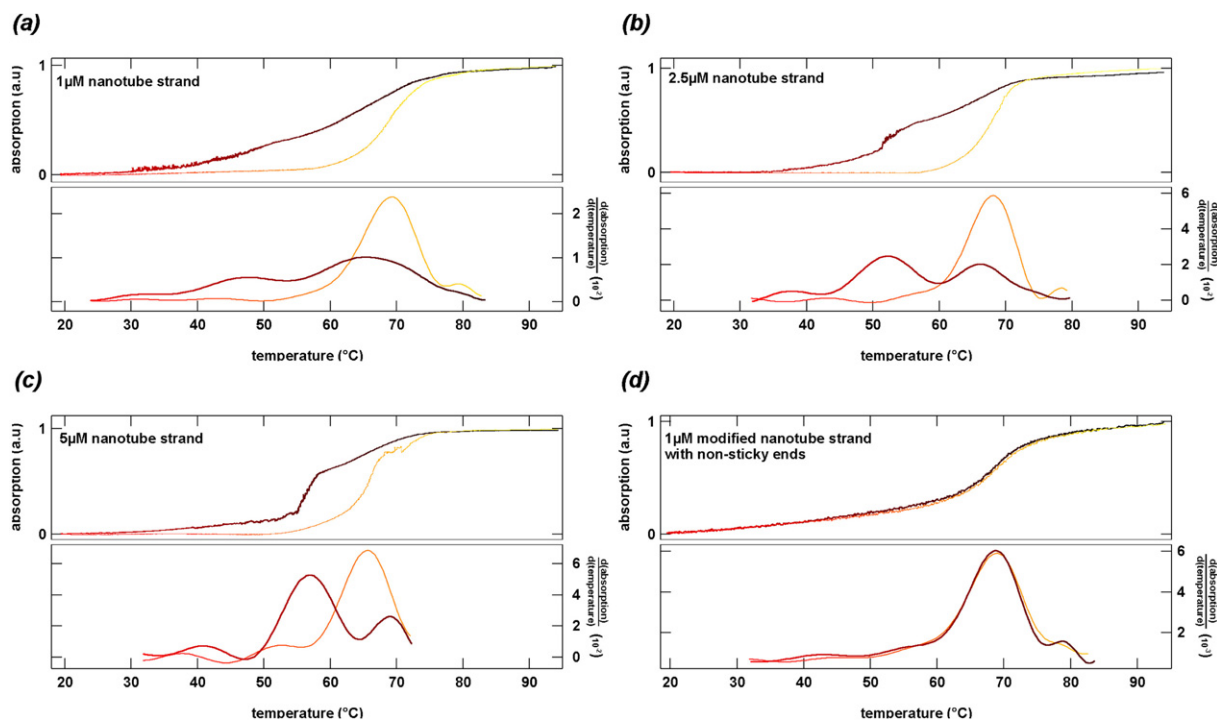


Figure 4. Formation (heavier line) and melting (lighter line) of DNA nanotubes in solution as measured by absorption at 260 nm. The lower graphs are differential absorption with respect to temperature (from fits to the data) illustrating formation/melting transitions. The formation process is clearly different to the melting process. (a) $1 \mu\text{M}$ concentration. (b) $2.5 \mu\text{M}$ concentration. (c) $5 \mu\text{M}$ concentration. (d) a modified DNA nanotube at $1 \mu\text{M}$ concentration with an identical number of bases but with ends (segments 1 and 4) which are not complementary, that is they should not hybridize. Thus it is expected that tiles form but no further development into lattices or nanotubes takes place. There appears to be only one transition at temperatures similar to the first transition in (a), confirming this hypothesis.

Photometrics, Arizona, USA) and processed using ImageJ software (National Institutes of Health, USA).

2.5. Transmission electron microscopy

A $3 \mu\text{l}$ drop of a sample solution was placed on a carbon-coated TEM grid (400 Mesh 3.05 mm copper, SPI Supplies, West Chester, PA). The drop was dabbed off with filter paper after 20 s followed by rinsing with H_2O . A $3 \mu\text{l}$ drop of 1% uranyl acetate negative staining solution was then placed on the grid for 20 s, dabbed off and left to dry for one hour. Imaging was performed with a JEOL JEM 100CX transmission electron microscope working at an accelerating voltage of 100 kV.

3. Results and discussion

Several sets of results are discussed. We show formation and melting curves of the nanotube solutions at different concentrations. Measurements of the individual segments are also presented for comparison, along with a modified strand that has the same number of nucleotides, but ends (segments 1 and 4) that are designed not to be complementary. The absorption curves of the nanotube solution are then compared with atomic force microscopy and fluorescent microscopy results, and the significance of these results is discussed.

UV absorption measurements can follow the assembly and melting of DNA structures because double-stranded DNA has a lower absorbance at 260 nm than single-stranded DNA

(hyperchromicity), so changes in absorbance are proportional to changes in the amount of unpaired DNA and slightly dependent on temperature [15]. Figure 4(a) shows the formation and melting curves at $1 \mu\text{M}$ strand concentration. The lower graph is a differential of absorption with temperature (numerically differentiated to a high order ($n = 100$) polynomial fit of the data). The hysteric cycle indicates kinetic barriers to nucleation. The formation process is not a two-state transition but has multiple intermediate states as indicated by the multiple peaks in the differential curve. The noise in the data at lower temperatures most likely arises from light scattering as the lattices form lattices of the order of the wavelength of light.

In comparison, a measurement of the DNA strand that is designed not to have complementary ends (segments 1 and 4) is plotted in figure 4(d). The formation and melting processes are reversible without hysteresis. This suggests that tiles are forming as expected—the inner segments 2 and 3 are each still self-complementary—and then no further assembly takes place because the tiles are unable to bind together. At 2.5- and 5-times higher concentrations, as shown in figures 4(b) and (c), an increasingly sharper second transition is observed in the formation process. The reason for this may be that at higher concentrations the tiles interact increasingly frequently and thus lattices form faster. Whether the lattices grow with the same quality is being further researched.

The melting processes all appear to exhibit two-state transitions of similar nature. They exhibit a single major

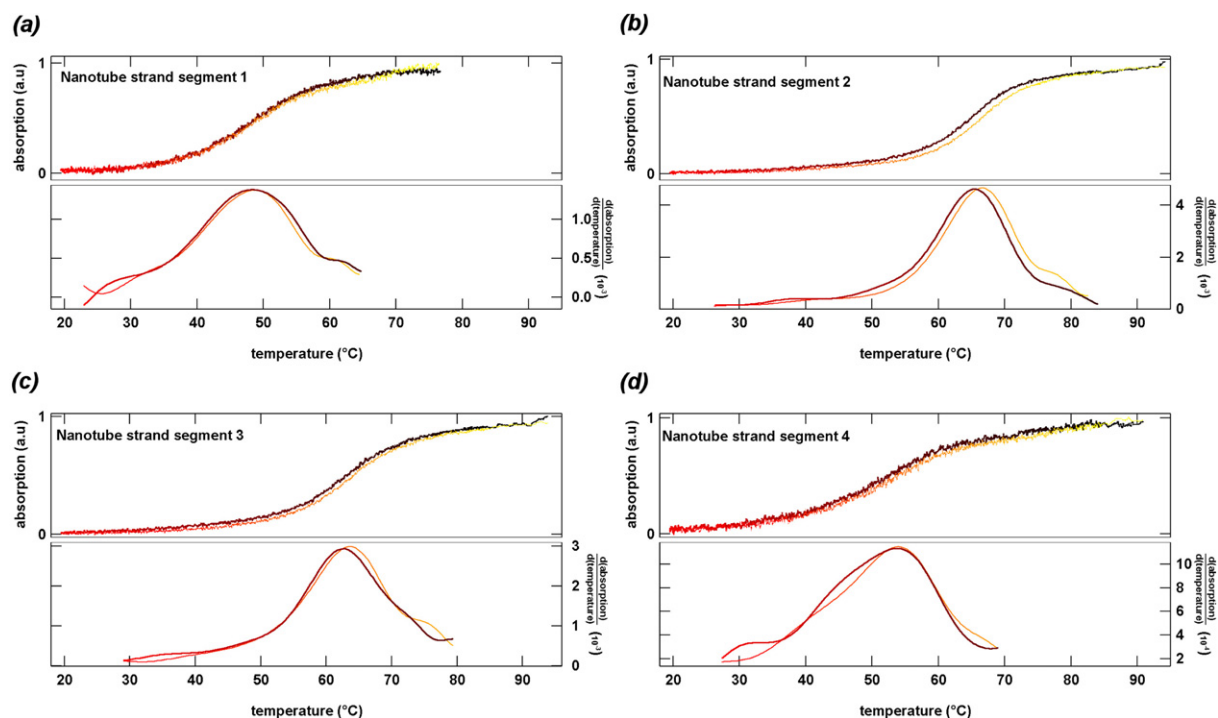


Figure 5. Hybridisation (heavier line) and melting (lighter line) of the individual palindromic segments that together compose the sequence used for the DNA nanotubes. Segments 2 and 3, the longer inner segments, which in the original sequence form the tile, have melting points close to the highest temperature peak observed in the differential of the formation of the tubes (figure 4(a)), which indicates this is the peak of tile formation. Segments 1 and 4 have higher melting points than the second temperature peak indicating that co-operativity effects are necessary for the lattice to form.

peak in the differential curve. It has to be noted that such a behaviour is only observed reproducibly when the DNA strands have been carefully assembled in a previous annealing step. In an untreated sample, the whole spectrum of partially assembled DNA strands is present (as indicated in figure 2), resulting in non-reproducible melting behaviour. Thus, initial annealing also serves to set a defined starting state for the melting experiments.

The hybridization and melting curves of the individual segments 1, 2, 3 and 4 at 1 μM concentration are shown in figure 5. These all appear to be reversible and with little or no hysteresis. The longer inner segments 2 and 3 have higher melting temperatures than the shorter ends. These are both close to the first transition observed in the formation of the 1 μM DNA nanotube strand sample and indicate that this is likely to be the inner segments hybridizing to form the double crossover tile as depicted in figure 1(b). The outer segments 1 and 4 are shorter and have a lower transition temperature. Hybridization of these shorter segments are responsible for lattice and nanotube formation which occur at lower temperatures.

Experiments were performed to directly observe the structures as formation and melting took place. A DNA nanotube solution was sampled at certain temperatures. The sample volumes were immediately put on ice to stop continued structure formation. The sample was then imaged within a few minutes in buffer with atomic force microscopy.

The formation results are shown in figure 6. The first image is of the mica surface without DNA solution. The

following images were sampled at the labelled temperature. At 70 $^{\circ}\text{C}$ very little can be identified: presumably most of the DNA is still single-stranded at this high temperature. Between 70 and 60 $^{\circ}\text{C}$ some structure forms: this is probably tiles as this corresponds to the temperature regime just after the first peak of the differential curve in figure 4(a). Between approximately 40 and 30 $^{\circ}\text{C}$ lattices begin to appear: this correlates with being just after the second peak in the differential curve. Below approximately 30 $^{\circ}\text{C}$ short nanotubes appear: this correlates with being just after the third peak in the differential curve. The tubes are relatively short compared to those in figure 3 because the annealing protocol was 12 h as opposed to 48 h. The correlation between the atomic force microscopy images and the UV absorption measurements thus provides evidence for a hierarchy in the nature of the nanotube assembly.

The reverse process of nanotube melting by heating the solution was also observed and the results are shown in figure 7. The solution was heated over 12 h from 20 to over 75 $^{\circ}\text{C}$. The nanotubes are stable until at least 60 $^{\circ}\text{C}$ and at 70 $^{\circ}\text{C}$ there is little sign of any remaining structure, while at 75 $^{\circ}\text{C}$ no structure is seen. This again correlates with the UV absorption results in figure 4(a), where in the melting process a single transition is seen between 60 and 75 $^{\circ}\text{C}$. This is in agreement with Mao *et al* who also measured UV absorption of a melting nanotube solution and saw no change until 60 $^{\circ}\text{C}$ [20].

Observations with fluorescent microscopy also support these measurements. DNA nanotube solution was pipetted into the PDMS chamber between glass slides and stored at 4 $^{\circ}\text{C}$ over night to allow the nanotubes to bind to the glass. This

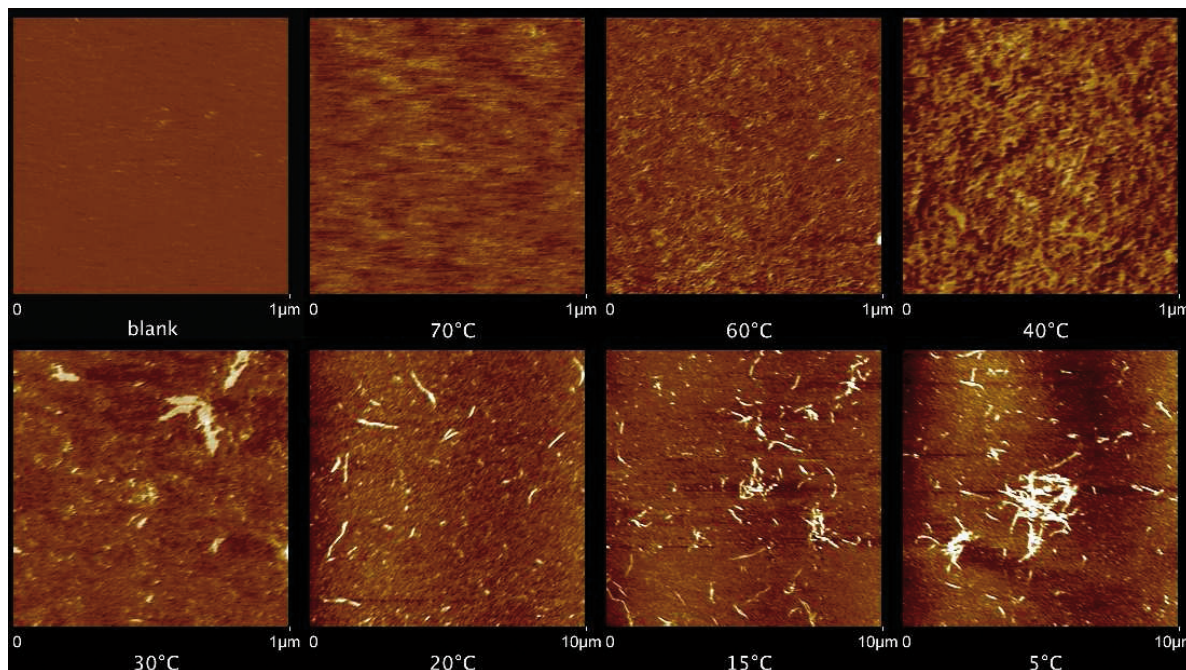


Figure 6. Atomic force microscopy images of a sequentially sampled DNA nanotube solution as it was cooled from 95 °C over 12 h. The first image is of a blank mica surface, following images are of samples taken at the indicated temperature. Height scale is 5 nm with lighter areas being higher. Several stages can be observed, initial binding of DNA (probably tile formation, resolution makes it difficult to clearly determine this) between 70 and 60 °C, lattice formation between ~40 and ~30 °C, and tube formation below ~30 °C. This correlates well with the UV absorption measurement of formation with the three peaks discernible in the formation differential in figure 4(a).

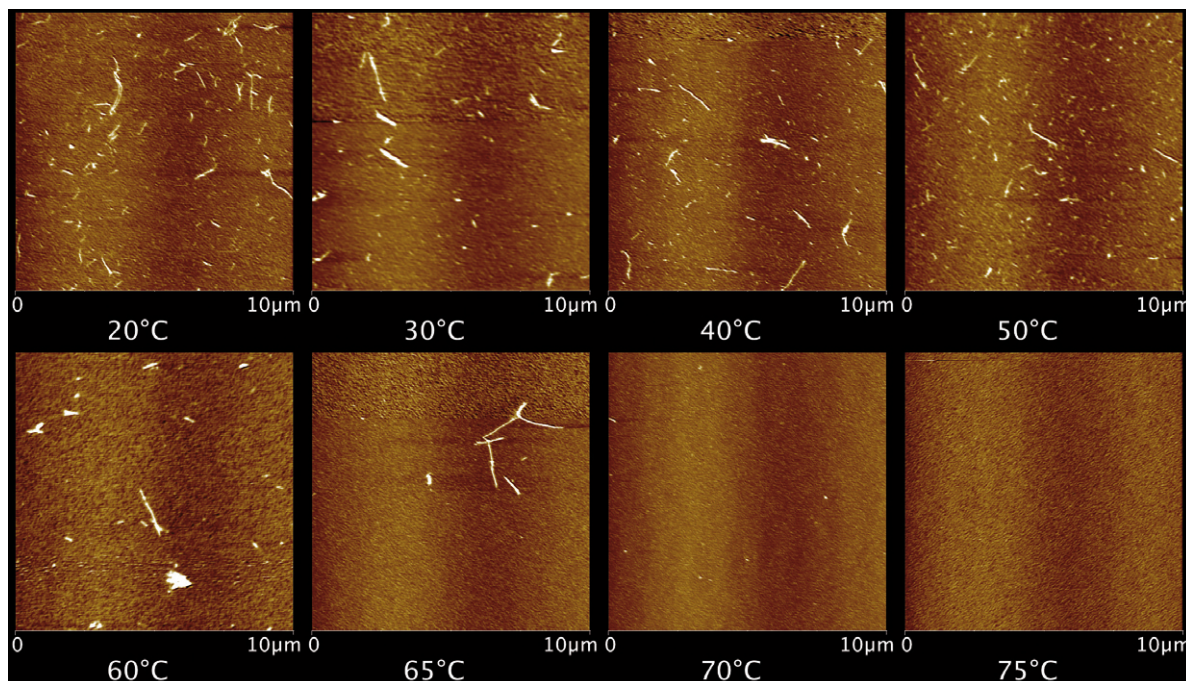


Figure 7. Atomic force microscopy images of a sequentially sampled DNA nanotube solution as it was heated from 20 °C over 12 h. Height scale is 5 nm with lighter areas being higher. The tubes appear to be stable to approximately 70 °C, and then melt rapidly above this temperature, no trace of them can be seen at 75 °C. This correlates well with the UV absorption measurement of melting with the single peak discernible in the melting differential in figure 4(a).

was then mounted on the microscope stage and heated while observing as described in section 2. The nanotubes in this case contained some (estimated 25%) DNA strands labelled

with fluorescein. Fluorescein is pH dependent and the TAE buffer does change pH with temperature, but it is sufficient for qualitative visual observation. The results are shown in

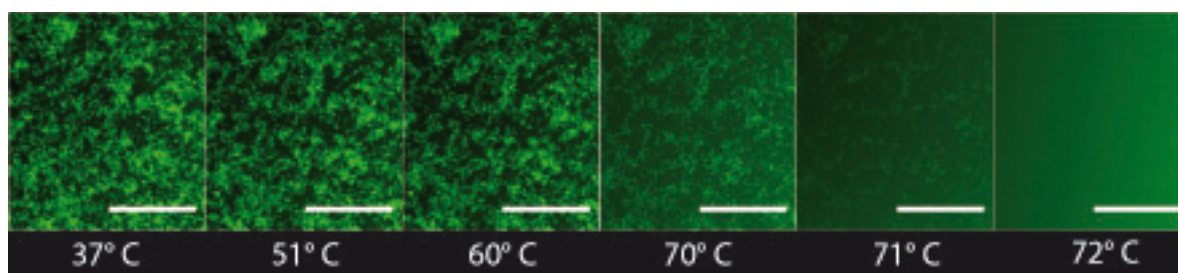


Figure 8. Low magnification fluorescent microscopy images of DNA nanotube solution. Individual tubes cannot be made out at this magnification: however, bulk behaviour of many tubes can be observed. The solution was heated *in situ* at $8\text{ }^{\circ}\text{C h}^{-1}$ and images were taken at the labelled temperatures. The scale bar is $200\text{ }\mu\text{m}$. The tubes appear to be stable to approximately $70\text{ }^{\circ}\text{C}$, and then melt within a few degrees of this temperature. This supports the UV absorption and atomic force microscopy measurements.

figure 8. Surface interactions with the glass may influence the stability of the nanotubes. However, it can be seen that the nanotubes appear to melt between 70 and $73\text{ }^{\circ}\text{C}$, supporting the results from UV absorption measurements and atomic force microscopy images.

The significant difference in formation and melting processes is important. It is not observed in recent experiments on two-dimensional assemblies demonstrated by Winfree [15]. These results show hysteresis but do not show a fundamental difference (as seen by the different shapes of the formation and melting curves supported by the AFM results) between formation and melting observed in the nanotube structure.

The reason for this difference is thought to result from a co-operative effect. Once the nanotubes are formed there are few non-paired strands exposed, only those at the ends of the nanotubes and those in any defects. The nanotubes are a ‘closed’ structure apart from the ends. In two-dimensional structures, the relative portion of non-paired strands is higher because of the relatively larger edges and because the structure is ‘open’. This higher portion of non-paired strands in an almost closed structure suggests that it is significantly more stable (i.e. melting at much higher temperatures) than two-dimensional lattices.

4. Conclusion

We have shown that a single, short and apparently simple DNA sequence can exhibit a rich spectrum of phenomena. Accurate thermodynamic predictions for DNA nano-assemblies are difficult due to the presence of multi-strand interactions. In the case of the DNA nanotubes studied here an additional complication arises from palindromic subsequences and pseudoknotted higher-order structures. Rather than fitting experimental data to standard thermodynamic and kinetic theories, we have correlated UV absorption measurements with atomic force microscopy and fluorescence microscopy. This has demonstrated the formation and melting of DNA nanotubes, illustrating important differences between these processes. The differences can be understood in terms of co-operativity between segments of the sequence and their binding and, when contrasted with results from two-dimensional self-assembly, indicate that closed three-dimensional structures may be significantly more thermodynamically stable.

Acknowledgments

We thank Helene Budjarek and Thomas Zeitzler for technical laboratory assistance, and Marianne Hanzlik for TEM assistance. We acknowledge support from the Nanosystems Initiative Munich. TLS acknowledges support from the International Doctorate Programme NanoBioTechnology at the Ludwig-Maximilians-Universität München and from the Elite Network of Bavaria. We thank Jörg P Kotthaus for use of his laboratories.

References

- [1] Liedl T, Sobey T L and Simmel F C 2007 *Nano Today* **2** 36–41
- [2] Feldkamp U and Niemeyer C M 2006 *Angew. Chem. Int. Edn* **45** 1856–76
- [3] Seeman N C 2007 *Mol. Biotechnol.* **37** 248–57
- [4] LaBean T H and Li H Y 2007 *Nano Today* **2** 26
- [5] Shih W, Quispe J and Joyce G 2004 *Nature* **427** 618–21
- [6] Rothmund P 2006 *Nature* **440** 297–302
- [7] Dirks R M, Bois J S, Schaeffer J M, Winfree E and Pierce N A 2007 *SIAM Rev.* **49** 65–88
- [8] SantaLucia J 1998 *Proc. Natl Acad. Sci. USA* **95** 1460–5
- [9] SantaLucia J and Hicks D 2004 *Annu. Rev. Biophys. Biomol. Struct.* **33** 415–40
- [10] Erie D, Sinha N, Olson W, Jones R and Breslauer K 1987 *Biochemistry* **26** 7150–9
- [11] Dimitrov R and Zuker M 2004 *Biophys. J.* **87** 215–26
- [12] Andronescu M, Zhang Z and Condon A 2005 *J. Microbiol.* **345** 987–1001
- [13] Dirks R and Pierce N 2004 *J. Comput. Chem.* **25** 1295–304
- [14] Bois J, Venkataraman S, Choi H, Spakowitz A, Wang Z and Pierce N 2005 *Nucleic Acids Res.* **33** 4090–5
- [15] Schulman R and Winfree E 2007 *Proc. Natl Acad. Sci. USA* **104** 15236–41
- [16] Sacca B, Meyer R, Feldkamp U, Schroeder H and Niemeyer C M 2008 *Angew. Chem. Int. Edn* **47** 2135–7
- [17] O’Neill P, Rothmund P W K, Kumar A and Fygenson D K 2006 *Nano Lett.* **6** 1379–83
- [18] Ekani-Nkodo A, Kumar A and Fygenson D 2004 *Phys. Rev. Lett.* **93** 268301
- [19] Jungmann R, Liedl T, Sobey T L, Shih W and Simmel F C 2008 *J. Am. Chem. Soc.* **130** 10062–3
- [20] Liu H P, Chen Y, He Y, Ribbe A E and Mao C D 2006 *Angew. Chem. Int. Edn* **45** 1942–5
- [21] Fu T and Seeman N 1993 *Biochemistry* **32** 3211–20
- [22] Rothmund P, Ekani-Nkodo A, Papadakis N, Kumar A, Fygenson D and Winfree E 2004 *J. Am. Chem. Soc.* **126** 16344–52

- [23] Liu D, Reif J and LaBean T 2003 *DNA Comput.* **2568** 10–21
- [24] O’Neill P 2005 *Biophys. J.* **88** 522A
- [25] Liu D, Park S, Reif J and LaBean T 2004 *Proc. Natl Acad. Sci. USA* **101** 717–22
- [26] Mitchell J, Harris J R, Malo J, Bath J and Turberfield A J 2004 *J. Am. Chem. Soc.* **126** 16342–3
- [27] Kuzuya A, Wang R, Sha R and Seeman N C 2007 *Nano Lett.* **7** 1757–63
- [28] Hou S, Wang J and Martin C 2005 *J. Am. Chem. Soc.* **127** 8586–7
- [29] Lin C, Ke Y, Liu Y, Mertig M, Gu J and Yan H 2007 *Angew. Chem. Int. Edn* **46** 6089–92